



Quasi-Spherical Brookite TiO₂ Nanostructures Synthesized Using Solvothermal Method in the Presence of Oxalic Acid

Yifei Wang^{1,4} · Yunling Zou^{2,3} · Qianqian Shang³ · Xin Tan⁵ · Tao Yu³ · Xianshou Huang¹ · Wenxin Shi² · Yao Xie² · Gao Yan² · Xiaoyi Wang²

Received: 18 February 2017 / Revised: 27 March 2017 / Accepted: 6 April 2017 / Published online: 29 November 2017
© The Author(s) 2017. This article is an open access publication

Abstract

Brookite TiO₂, the latest TiO₂ photocatalyst, promises to be an interesting candidate for photocatalytic applications because of its unique physical and chemical properties. In this study, pure-phase brookite TiO₂ with a quasi-spherical nanostructure was successfully synthesized via a solvothermal method using tetrabutyl titanate (Ti(OC₄H₉)₄, TBOT) as the Ti source in the presence of oxalic acid. NaOH was used to regulate the pH of solution. The structure and morphology of the samples were then analyzed using multiple methods, such as X-ray diffraction (XRD), Raman spectroscopy, scanning electron microscopy (SEM), transmission electron microscopy (TEM), Brunauer–Emmett–Teller (BET) measurements and ultraviolet–visible diffuse spectroscopy (UV–Vis). Photocatalytic activities of the as-synthesized brookite TiO₂ were evaluated by degrading aqueous methylene blue solution under UV light irradiation. The effect of thermal treatment temperature on photocatalytic activity of the samples was also investigated. The produced brookite TiO₂ nanopowders calcined at 500 °C for 2 h showed the highest photocatalytic activity, and the corresponding degradation rate of methylene blue (10 mg/L) reached 96.7% after 90 min of illumination. In addition, the formation mechanism of pure-phase brookite TiO₂ was investigated. It was found that the formation of pure-phase brookite TiO₂ in this study was ascribed to the combined action of oxalic acid and sodium hydroxide.

Keywords TiO₂ · Brookite · Oxalic acid · Photocatalytic properties

Introduction

It is known that TiO₂ shows three types of crystalline polymorphs: rutile (tetragonal, space group: *P42/mnm*), anatase (tetragonal, space group: *I41/amd*), and brookite (orthorhombic, space group: *Pbca*) [1]. Of these polymorphs, anatase and rutile TiO₂ have been widely studied over the past decades. However, few reports have focused on

the preparation and properties of brookite TiO₂, due to the difficulty involved in preparing its pure form [2–4]. Nevertheless, theoretical studies have demonstrated that brookite TiO₂ exhibits superior photocatalytic performance compared to anatase and rutile TiO₂ because of its unique orthorhombic crystalline structure [5–7]. Thus, brookite TiO₂ has generated significant interest due to its physicochemical properties and possible applications.

To date, various methods have been developed to synthesize pure brookite TiO₂, such as hydrothermal [8–12], sol–gel [13, 14], thermal decomposition [15] and solvothermal [16] methods. For example, Brookite TiO₂ derived from hydrothermal/solvothermal treatment of titanium complexes has been widely reported, and this is known to be an effective strategy for synthesizing pure-phase brookite TiO₂ [9–21]. Additionally, brookite TiO₂ nanoparticles have been prepared via hydrolysis of titanium (IV) isopropoxide at room temperature using isopropanol as both the solvent and the ligand [13]. The Koji group synthesized brookite TiO₂ via the hydrothermal treatment of different water-soluble

✉ Yunling Zou
zouyunling1999@126.com

¹ School of Environmental Science and Engineering, Tianjin University, Tianjin 300072, China

² College of Science, Civil Aviation University of China, Tianjin 300300, China

³ School of Chemical Engineering and Technology, Tianjin University, Tianjin 300072, China

⁴ Tianjin Metro Group Co., Ltd., Tianjin 300051, China

⁵ School of Science, Tibet University, Lhasa 850000, China

titanium complexes using hydroxyacetic acid, glycolic acid, citric acid, or ethylenediaminetetraacetic acid (EDTA) as complexing agents [9–12]; they concluded that the structures of titanium complexes were important for forming brookite TiO₂.

It is worth mentioning that oxalic acid is a rigid bidentate ligand that can link two metallic centers, and is a good chelating agent that effectively chelates with metal ions, including a titanium ion [17, 22, 23]. The decomposition of oxalate groups is primarily bi-coordinated or mono-coordinated to titanium atoms via a reaction with Ti–OH groups, which results in the evolution of CO, CO₂ and a minor amount of H₂O [14]. In addition, the titanium oxalate complex, which has a specific octahedral arrangement that is similar to the titanium glycolate complex, facilitates the growth of brookite TiO₂ polymorph with a high pH value [12, 19, 21]. Dambournet et al. [15] reported that mesoporous brookite TiO₂ with a high specific surface area and controllable morphology could be synthesized using titanium oxalate hydrate as a precursor in the presence of alkali ions (Li⁺, Na⁺). It is thus known that oxalic acid can be used to prepare brookite TiO₂ nanostructures with excellent properties. However, due to the strong dependence of brookite TiO₂ formation on the synthesis method and experimental conditions involved, more research is required to understand brookite TiO₂ formation under different conditions.

In this study, brookite TiO₂ was synthesized via the solvothermal method using tetrabutyl titanate (TBOT) as a Ti source and oxalic acid as a complexing agent. *N,N*-dimethylformamide (DMF) was used as a solvent, and the pH value of the solution was maintained at 10 by adding 2 mol/L NaOH. X-ray diffraction (XRD), Raman spectroscopy, field emission scanning electron microscopy (FESEM), high-resolution transmission electron microscopy (HRTEM), Fourier transform infrared spectroscopy (FTIR), and ultraviolet–visible diffuse spectroscopy (UV–Vis) were employed to characterize the structure and morphology of the products. The photocatalytic activity of the produced brookite TiO₂ was evaluated by photodegrading methylene blue (MB) solution under UV light irradiation. In addition, this work investigated the formation mechanism of brookite TiO₂ in the presence of oxalic acid during the solvothermal process.

Experimental

Materials

Tetrabutyl titanate (Ti(OC₄H₉)₄, TBOT) of analytical grade was purchased from Sinopharm Chemical Reagent Co., Ltd., China. Analytical-grade sodium hydroxide (NaOH),

oxalic acid (H₂C₂O₄·2H₂O), *N,N*-dimethylformamide (DMF), sodium sulfate (Na₂SO₄), absolute ethanol, 2-propanol (IPA), and EDTA disodium salt (EDTA-2Na) were purchased from Kewei Company of Tianjin University, China. All chemicals were directly used without further purification.

Synthesis of Brookite TiO₂ Nanostructures

In total, 1.27 g of oxalic acid was first dissolved in 50 mL of DMF solution via vigorous stirring, and 1.0 mL of TBOT was then slowly dropped into the mixture. Vigorous stirring was applied until a transparent yellow solution was formed. The pH value of the resulting solution was adjusted to 10 using 2.0 mol/L NaOH during this process. The solution was then stirred for another 1 h, and the slurry formed was transferred to a 100 mL Teflon-lined autoclave and placed in an oven at 180 °C for 8 h. It was then slowly cooled to room temperature, and the white precipitate was subsequently collected using centrifugation. The precipitate was washed several times with distilled water and absolute ethanol and then dried at 80 °C overnight in a drying cabinet.

Characterization

The crystalline phase, phase composition, and crystallite size of the product were characterized using powder XRD via a DX-2000 X-ray diffractometer with CuK α radiation at a scan rate of 0.06°/s. The accelerating voltage and applied current were 35 kV and 25 mA, respectively. The average TiO₂ sample crystallite size (*D*) was calculated from X-ray line broadening of reflections of the three main peaks using the Scherrer equation.

The morphologies and particle sizes of prepared TiO₂ powders were examined using an FESEM (Hitachi, S-4800), and the detailed microscopic nanostructure was observed using a HRTEM (JEOL, JEM 2100F operated at 200 kV). Raman spectra were recorded using a DXR Microscope Raman spectrometer system with an excitation wavelength of 532 nm at room temperature. Nitrogen adsorption–desorption measurements were taken at 77 K using a Micromeritics TriStar nitrogen adsorption apparatus (Micromeritics Instrument Corporation, USA). The samples were degassed at 300 °C for 4 h prior to Brunauer–Emmett–Teller (BET) measurements, and the BET surface areas, *S*_{BET}, were calculated within the relative pressure range of 0.05 to 0.20. Desorption isotherms were used to determine the pore-size distribution via the Barrett–Joyner–Halenda (BJH) method. UV–Vis diffuse reflectance spectra were recorded using a UV–visible spectrophotometer (UV-2600, Shimadzu, Japan) and then converted into absorption spectra via Kubelka–Munk transformation.

Photoelectrochemical Evaluation

The electrochemical performance of brookite TiO₂ was evaluated at a CHI660E electrochemical workstation (Shanghai Chenhua Instrument Co., China). Electrochemical measurements were taken using a conventional three-electrode configuration with an as-prepared brookite TiO₂/FTO employed as the working electrode (1 cm × 1 cm), a Pt wire as the counter electrode, and a Ag/AgCl electrode as the reference. The working electrode of TiO₂/FTO was prepared according to the method reported in our previous work [24]. The electrodes were placed 3 cm apart, and the supporting electrolyte was 0.1 mol/L Na₂SO₄ solution. Electrochemical impedance spectroscopy (EIS) measurements were taken in the frequency range of 100–0.01 Hz using amplitude of 5 mV and an open-circuit potential without illumination. The flat band potential (E_{FB}) of the samples was determined from Mott–Schottky (M–S) analysis at an alternating-current potential frequency of 1 kHz under dark conditions.

Photocatalytic Performance Test

The photocatalytic performance of brookite TiO₂ powders was evaluated using the photodegradation of an aqueous solution of MB. A Xenon lamp (HXS-F/UV 300, Beijing NBET Technology Co., Ltd) with a 365-nm band filter served as the light source and was placed 10 cm away from the liquid surface, where the light density was approximately 10 MW/cm. An appropriate amount of photocatalyst (15 mg) was added into 75 mL of MB solution (10 mg/L). To equilibrate the adsorption and desorption, the suspension was stirred in the dark for 30 min prior to UV illumination. Samples were periodically collected and centrifuged, and the concentration of the MB solution was analyzed using a UV–Vis spectrophotometer (T6, China).

To determine the effect of active species generated by the photocatalytic system on the photocatalytic activity of samples, various scavengers, including 2-propanol (IPA, 20 mmol/L) and EDTA-2Na (6 mmol/L), were introduced into the MB solution.

Results and Discussion

XRD, Raman, and FTIR Analyses

The crystalline structures of brookite TiO₂ synthesized via the solvothermal method in the presence of oxalic acid at 180 °C for 8 h were confirmed using XRD patterns and indexed using the Joint Committee on Powder Diffraction Standards (JCPDS), as shown in Fig. 1a.

All peaks of the sample synthesized in the presence of oxalic acid were confirmed to show the orthorhombic crystal structure of brookite TiO₂ (PDF# 29-1360). There were no other characteristic peaks observed belonging to impurities or other TiO₂ polymorphs (anatase and rutile), which indicated that the sample was pure-phase brookite TiO₂. To investigate the effect of oxalic acid on brookite phase formation, another sample was synthesized under the same solvothermal conditions in the absence of oxalic acid and was found to be titanic acid (H₂Ti₂O₅·H₂O; PDF# 47-0124) instead of brookite TiO₂ (as shown in Fig. 1a) [9]. This result indicates that oxalic acid plays an important role in the crystallization and phase formation of brookite TiO₂. However, oxalic acid is not the sole factor influencing the phase formation of pure brookite; a different crystal phase (pure anatase, pure rutile, or anatase–brookite biphas) TiO₂ was synthesized at a different pH value when oxalic acid was used as a chelating agent [17, 19]. It is thus concluded that brookite formation in this study is primarily attributed to the synergistic effect between oxalic acid and sodium hydroxide.

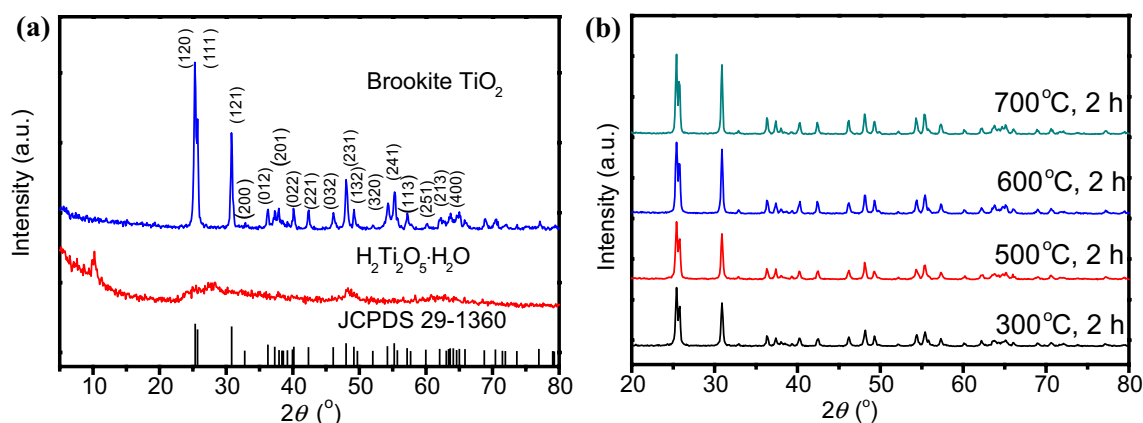


Fig. 1 XRD patterns of the samples **a** synthesized in the presence or absence of oxalic acid and **b** synthesized in the presence of oxalic acid and calcined at different temperatures

In addition, the pure brookite phase is only obtained under mild alkaline conditions, and titanate is formed when the pH value of the solution is higher than 10 [25].

The thermal phase stability of synthesized brookite TiO₂ was investigated by annealing the sample at different temperatures for 2 h, as shown in Fig. 1b. No phase transition was observed in the XRD patterns, even at a calcination temperature of 700 °C, which indicates that brookite TiO₂ synthesized under the present conditions possesses good thermal stability. The average crystallite sizes of samples without calcination and those calcined at 300, 500, 600 and 700 °C were calculated using Scherrer equation, and the (121) peaks were found to be 27.65, 28.32, 31.86, 33.02, and 35.93 nm, respectively. This result reveals that the thermal treatment temperature has no influence on the phase structure or composition of the samples and it only affects crystal size.

Raman spectroscopy is a sensitive technique used to confirm the existence of pure brookite in a sample, where the lower symmetry and larger unit cell of brookite result in a larger number of Raman and infrared-active phonons compared to anatase and rutile structures [26]. The relatively complex vibrational spectrum includes a stretching vibration (Ti–O) and a flexural vibration (Ti–O–Ti) [8], and the two types of O atoms that exist in brookite make all the bond lengths between the titanium and oxygen atoms different [1]. Figure 2 shows the Raman spectra of the as-synthesized brookite TiO₂ powders without calcination and those calcined at 500 °C, respectively. The detected Raman vibration peaks are indexed as A_{1g} (127, 152, 194, 246, 324, 412, 545 and 640 cm⁻¹), B_{1g} (212 and 283 cm⁻¹), B_{2g} (366, 460 and 542 cm⁻¹), and B_{3g} (500 cm⁻¹) [26, 27]. Raman peaks are thus in good agreement with the Raman-active modes of brookite TiO₂. As no characteristic peak belonging to anatase TiO₂ exists at 516 cm⁻¹, it is suggested that the samples are pure brookite, and that chelation of C₂O₄²⁻ with

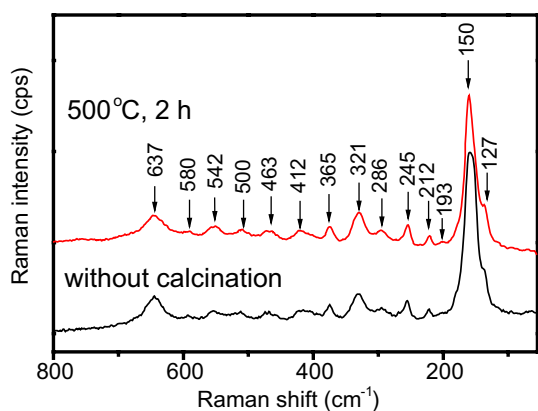


Fig. 2 Raman spectra of brookite TiO₂ nanopowders without calcination and those calcined at 500 °C

different types of O atoms results in the formation of distorted TiO₆ octahedron that facilitates the growth of brookite crystallites. The Raman spectra of brookite TiO₂ calcined at 500 °C are also presented in Fig. 2, and no phase transition is observed. This result is in agreement with results of XRD. One possible explanation for the thermal stability is the correlation between surface enthalpies and the brookite TiO₂ crystalline size. The energies of anatase, brookite, and rutile are sufficiently close to be reversed by small differences in surface energies. Zhang and Banfield [28] demonstrated that brookite is more stable than anatase for crystal sizes greater than 11 nm, while rutile is the most stable phase for sizes greater than 35 nm. All of the crystal sizes synthesized are within this reference range.

SEM and TEM Analyses

To confirm the morphological features of the as-obtained TiO₂ powders calcined at different temperatures, the samples were further characterized using FESEM and HRTEM. Figure 3a–e shows SEM images of samples without calcination and those calcined at 300, 500, 600 and 700 °C. It can be observed that brookite TiO₂ without calcination exhibits quasi-spherical structures (Fig. 3a), which consist of many smaller particles measuring approximately several nanometers in diameter. After calcination at 300 °C, the quasi-spherical structures with a rough surface are improved, as shown in Fig. 3b; this is attributed to an improvement in crystallinity. The surface of the spherical structures changes from rough to smooth, and the grain size increases with an increase in the calcination temperature, as shown in Fig. 3c–e. This indicates that the product is sintered when the calcination temperature exceeds a certain value.

To further investigate the crystal morphology, TEM and HRTEM analyses were conducted to confirm the quasi-spherical TiO₂ structures, as shown in Fig. 3f–i. Figure 3f shows the TEM image of brookite TiO₂ without calcination, which confirms the existence of abundant quasi-spherical nanoparticles with an average particle size of approximately 20–40 nm. It is in good agreement with results from the SEM image (Fig. 3a) and the crystallite size calculated using Scherrer equation. With an increase in the calcination temperature, the diameters of the quasi-spherical structures increase (Fig. 3g, h); this is attributed to agglomeration of the nanoparticles during the thermal treatment process. Moreover, a large number of white dots are observed on the surface of the quasi-spherical structures, as shown in Fig. 3h, which indicates that the sample calcined at 500 °C exhibits a porous structure resulting from an improvement in crystallinity and the accumulation of small particles, and it is consistent with results from the SEM image shown in Fig. 3c. The HRTEM image of a typical quasi-spherical structure is shown in Fig. 3i, and the distinct lattice spacing

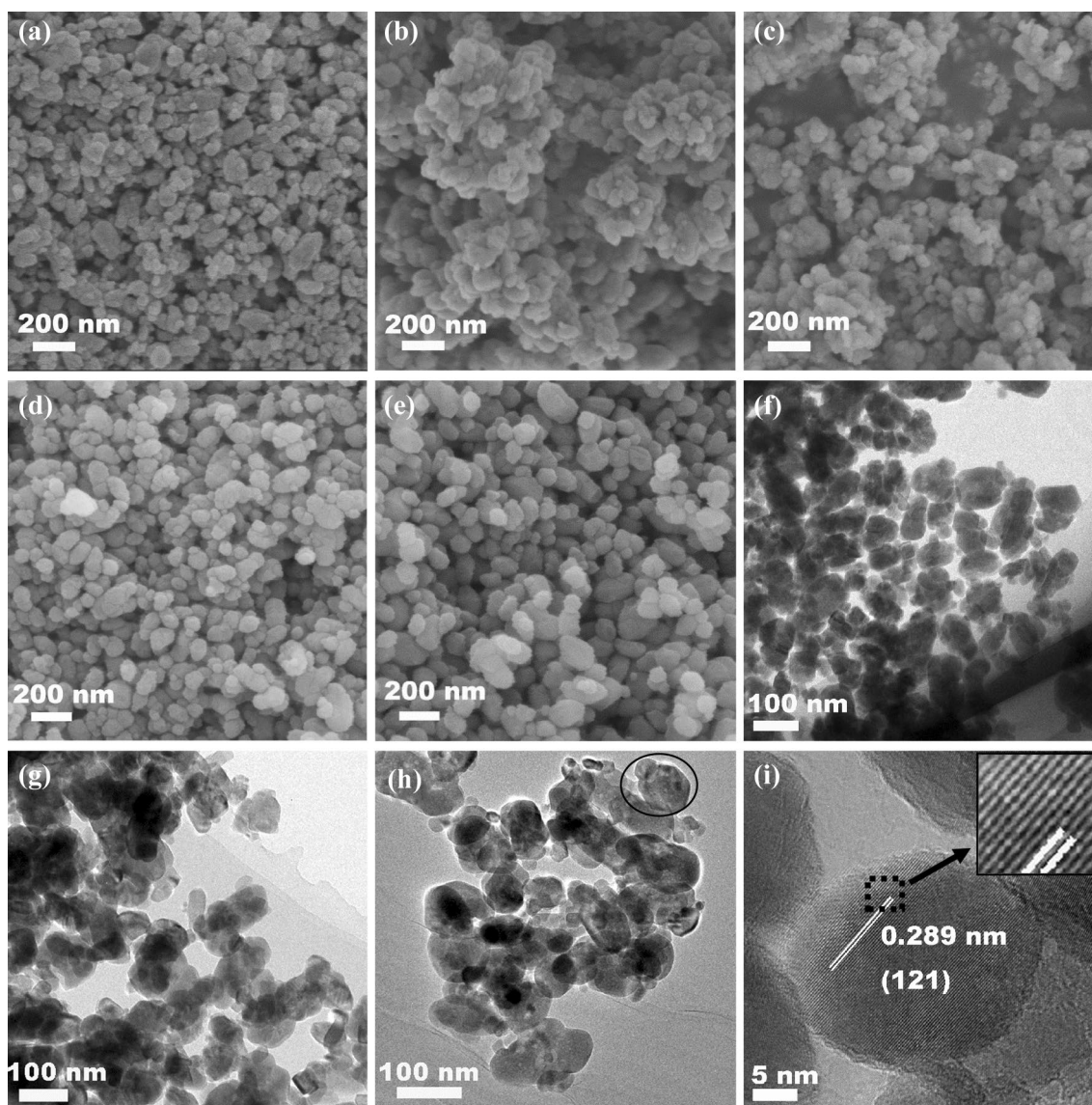


Fig. 3 SEM and TEM images of brookite TiO_2 **a, f, i** without calcination and TiO_2 calcined at different temperatures: **b, g** 300 °C, **c, h** 500 °C, **d** 600 °C and **e** 700 °C

of 0.289 nm between the adjacent lattice planes is attributed to the (121) crystal plane.

BET Analysis

Figure 4 shows the nitrogen adsorption–desorption isotherms and pore-size distribution curves of prepared TiO_2 powders calcined at various thermal treatment temperatures. It is observed from Fig. 4a that all synthesized samples show a typical Brunauer–Deming–Deming–Teller (BDDT) type-IV curve. At a high relative pressure range between 0.8 and 1.0, all curves exhibit clear hysteresis loops, which indicates the presence of a mesoporous structure (2–50 nm).

The N_2 adsorption–desorption isotherms at a high relative pressure, as shown in Fig. 4a, show that the hysteresis loop area increases with an increase in the calcination temperature. It indicates that the calcination temperature has an important influence both on the BET specific surface area and on the average pore size. The average pore sizes were calculated using the Barrett–Joyner–Halenda (BJH) model derived from the desorption branches of isotherms. BET surface area values and average pore sizes are presented in Table 1; it is evident that the BET surface areas of samples change as the calcination temperature increases, which is attributed to the porous structure of the samples resulting from decomposition of the oxalate precursor. The average pore size of samples increases with an increase in the

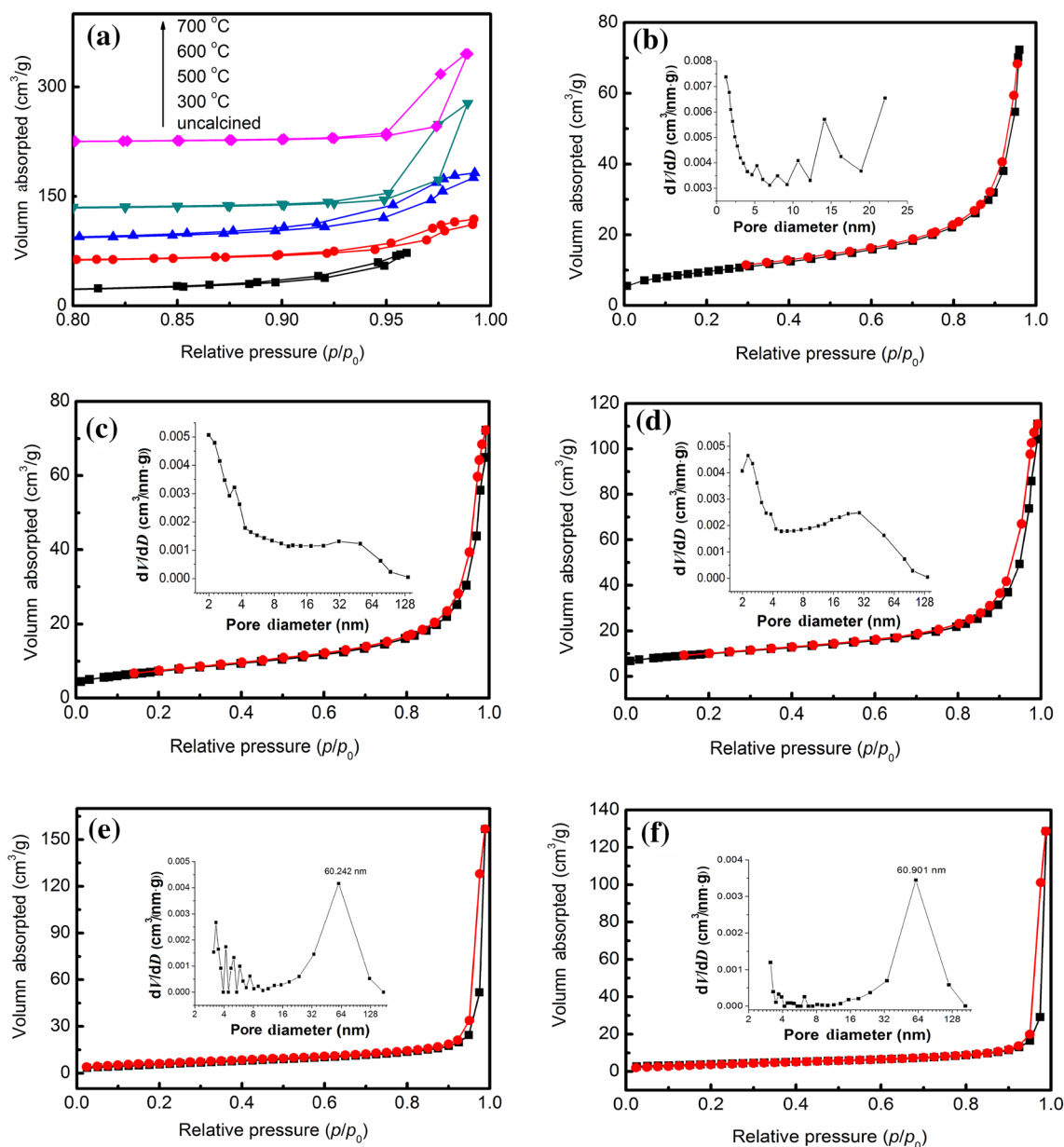


Fig. 4 N₂ adsorption–desorption isotherms of brookite TiO₂ nanospheres calcined at various temperatures for 2 h **a** comparison diagram of N₂ adsorption–desorption isotherms at high relative pressure,

b without calcination, **c** 300 °C, **d** 500 °C, **e** 600 °C, **f** 700 °C. The insets are their respective pore-size distribution patterns

Table 1 BET surface area and pore-size distribution of samples

Calcination temperature (°C)	Crystal size (nm)	S _{BET} (m ² /g)	Average pore size (nm)	Pore volume (cm ³ /g)	BJH desorption (nm)
–	27.65	34.3	13.05	0.112	13.1
300	28.32	26.4	10.23	0.112	16.0
500	31.86	35.4	12.87	0.114	18.6
600	33.02	22.62	42.87	0.241	60.24
700	35.93	14.61	54.48	0.199	60.90

calcination temperature; this is related to the compacted structure and the improved crystallinity due to the increase in calcination temperature. In addition, more than one peak in the pore-size distribution is observed, as shown in the insets of Fig. 4b–f, which indicates that the as-prepared TiO₂ has a hierarchically porous structure.

Possible Mechanism for Growth of Brookite TiO₂ in the Presence of Oxalic Acid

In recent years, brookite TiO₂ nanostructures (synthesized via thermal treatment of titanium complexes derived from different Ti sources and complexing agents) have been widely reported, and their corresponding growth mechanisms have been investigated [15–20]. Some researchers have suggested that a ligand type is crucial to TiO₂ phase formation during the hydrothermal treatment process, because ligand may coordinate to titanium in an octahedral environment and be assembled into the initial structure of anatase, brookite, or rutile crystallites [9–12, 21, 29–32]. In general, in an aqueous medium, titanium cations are solvated and form 6-coordinate charged complexes [TiL₆]^{z+}, in which the nature of the ligand (L) is indicated by the solution pH and the presence of species that act as complexing agents [29].

Oxalic acid is a rigid bidentate ligand; it is a good chelating agent that has been used to synthesize TiO₂. However, no consensus currently exists about the effect of oxalic acid on TiO₂ phase formation. For example, Dambournet et al. [22] reported that the [C₂O₄²⁻]/[Ti⁴⁺] molar ratio (denoted as *R*) was the key factor in TiO₂ phase formation and that the oxalate anion either acts as a ligand to stabilize the oxalate hydrate phase Ti₂O₃(H₂O)₂(C₂O₄)·H₂O (*R* = 1) before the formation of brookite TiO₂ after thermal treatment, or acts as a chelating agent (*R* = 2) to stabilize the rutile phase. However, Kanna and Wongnawa [30] suggested that oxalic acid inhibited the formation of rutile because the bi-bonds of C₂O₄²⁻ on the TiO₆ octahedra occupy one full octahedral face and inhibit the growing chain along opposite edges. Truong et al. [19] proposed that the presence of oxalic acid in solution prevented anatase formation through its chelation to the TiO₆ octahedron at the bridging oxo group, which benefited the growth of rutile crystallites. However, the results obtained in this study differed from the reported results when using oxalic acid as a complexing agent. Specifically, pure-phase brookite TiO₂ instead of rutile was obtained under solvothermal conditions with *R* > 2, which indicated that brookite TiO₂ derived from the titanium oxalate phase could be obtained with higher oxalate content by tuning other synthesis conditions. It can thus be inferred that the formation of brookite TiO₂ is related to the existence of NaOH, which is introduced to

maintain the pH value at approximately 10. Dambournet et al. [15] reported that the titanium oxalate phase played an important role in the morphology and crystallization of TiO₂ due to the type of preferentially adsorbed alkali ions (Li⁺, Na⁺) on its crystal facets. The three crystal forms of TiO₂, including anatase, rutile, and brookite, are composed of a [TiO₆] octahedron that has oxygen ions at its vertices and titanium atoms at its center; these have different spatial arrangements that share edges and corners in different manners. The [TiO₆] octahedral structure prefers corner sharing to edge sharing to maintain its thermodynamic stability, because the repulsive Coulomb forces that result from the shared edges lead to a decrease in stability [33]. Therefore, it is here considered that the addition of oxalic acid and NaOH changes the spatial arrangement of the [TiO₆] octahedron, which results in the formation of brookite TiO₂. Na⁺ ions have been reported to favor the brookite transition because they retard the collapse of layers due to stronger electrostatic interactions with titanate layers and induce the phase transition of titanate into brookite TiO₂ [34]. In addition, it has been reported that the pH value of solution significantly influences the TiO₂ crystalline structure [3]; a high pH supports edge-shared bonding (anatase crystallization), while a low pH favors corner-shared bonding (rutile crystallization). Brookite has both shared edges and corners and is midway between anatase and rutile in terms of edge-shared bonding, and at a low NaOH concentration, OH⁻ deficiency leads to the formation of [TiO₆] octahedra with brookite rather than anatase.

To further investigate the effects of oxalic acid and NaOH on brookite TiO₂ formation, a sample was synthesized using the same solvothermal conditions in the absence of oxalic acid. The XRD result in Fig. 1a demonstrates that titanite instead of brookite TiO₂ was obtained. Therefore, we conclude that the formation of brookite TiO₂ is a result of the combined action of oxalic acid and NaOH, and the possible mechanism involved in this process can be deduced. Specifically, the bond between ligands and the Ti precursor is fragile in a high pH solution and is readily cleaved because of the frequent nucleophilic attack on Ti atoms from abundant hydroxide ions. Thus, hydrolysis and condensation occur primarily along the edge-sharing bonds, which results in the formation of anatase and brookite crystallites. Therefore, the action of oxalic acid and the adjustment of pH value with sodium hydroxide are the main factors involved in forming pure brookite TiO₂.

We thus propose that the formation mechanism of brookite TiO₂ under the current experimental conditions is related to four processes: (1) the formation of Ti–OH groups derived from the tetrabutyl titanate hydrolysis reaction, (2) the complexation reaction between the oxalate ligands and the Ti–OH groups via the bi-coordination process, (3) the

transformation of titanium oxalate-based compound with the addition of NaOH, and (4) the formation of brookite TiO₂ under solvothermal conditions, including a high pH value (pH 10), which is described in Fig. 5.

UV-Vis Spectra

The diffuse absorbance spectra of as-synthesized brookite TiO₂ were analyzed using a UV-Vis spectrophotometer, as shown in Fig. 6a. The absorption edges were estimated to be 367.3, 364.4, 364.0, 363.6 and 363.9 nm for samples without calcination and those calcined at 300, 500, 600 and 700 °C, respectively. A slight blueshift occurs with an increase in calcination temperature. The optical band gap (E_g) of as-synthesized brookite TiO₂ was determined using Eq. (1):

$$\alpha h\nu = A(h\nu - E_g)^n, \quad (1)$$

where α is the linear portion of the absorption coefficient; $h\nu$ is photon energy; and A is a constant [35]. As brookite TiO₂ is an indirect band gap semiconductor, the value of n is determined to be 2. The plots of $(\alpha h\nu)^{1/2}$ versus $h\nu$ from the spectral data in Fig. 6a are presented in Fig. 6b–f. Extrapolation of the linear parts of the curves yields indirect band gaps of 2.939, 3.313, 3.330, 3.335 and 3.338 eV for samples without calcination and those calcined at 300, 500, 600 and 700 °C, respectively. Di Paola et al. [36] reported

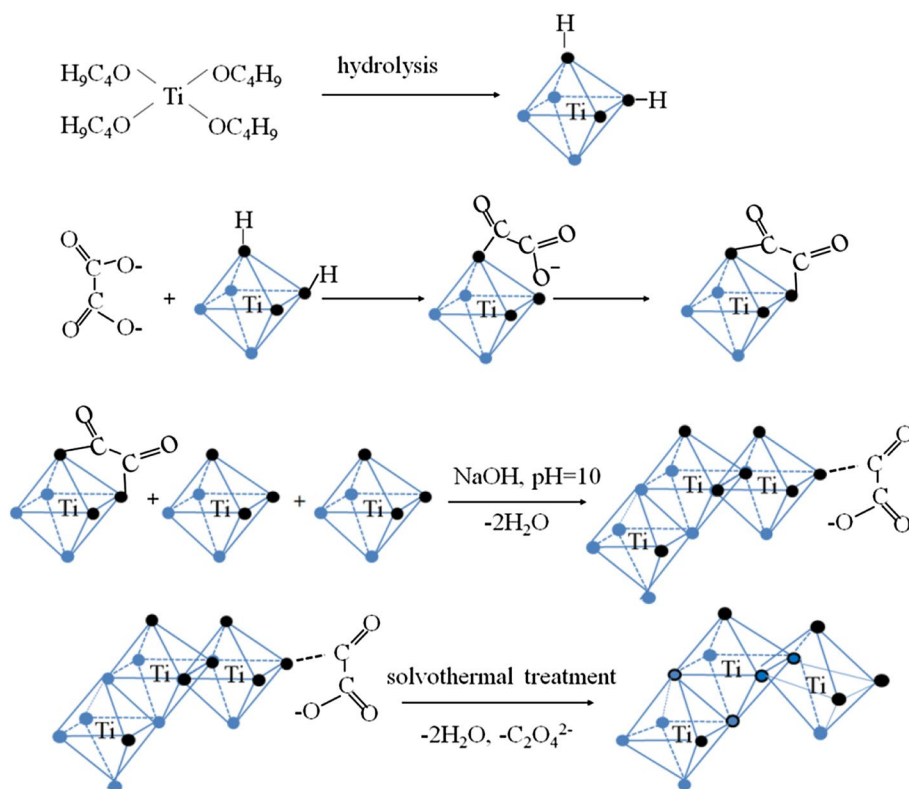
that an increased band gap corresponds to a more powerful redox ability, which contributes to enhanced photocatalytic activity. It is thus concluded that the photocatalytic activity of the samples is improved after calcination.

Photoelectrochemical Analysis

It is known that the photocatalytic activity of TiO₂ depends on its structure and physical properties [37]. Examination of electrochemical impedance spectroscopy (EIS) and flat band potential (E_{FB}) of the brookite TiO₂/FTO electrodes may be helpful in understanding the relationship between the photocatalytic activity of brookite TiO₂ and its physical properties.

EIS is an effective approach for investigating the capacitance and resistance of electrode materials and has been used to investigate the electrochemical properties of brookite TiO₂. EIS measurements were taken in a 0.1 mol/L Na₂SO₄ solution at an AC frequency from 100 kHz to 0.1 Hz without irradiation; results of EIS are presented in Fig. 7a in the form of Nyquist plots. It was found that the impedance arc diameter of brookite TiO₂ first sharply decreased as the calcination temperature increased below 500 °C and then increased when the calcination temperature reached higher than 500 °C. This indicates that the electron-transfer rate from the electrolyte to the electrode surface is enhanced by the increasing calcination temperature below 500 °C, which

Fig. 5 Schematic illustration of the brookite TiO₂ formation via solvothermal method in the presence of oxalic acid



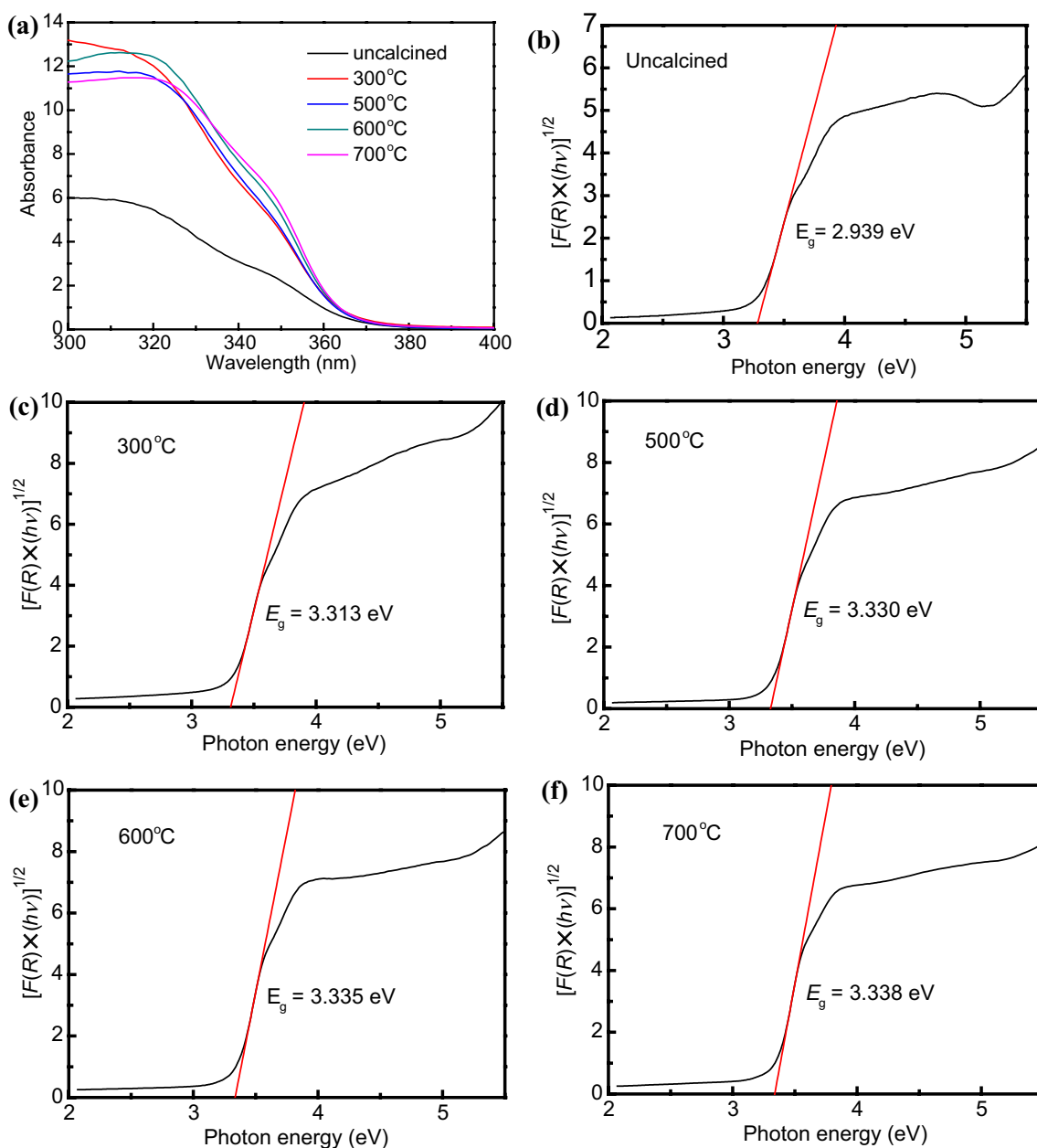


Fig. 6 a UV-Vis diffuse reflectance spectra; and b–f plots of modified Kubelka–Munk function versus energy of light absorbed by brookite TiO₂ calcined at different temperatures

is attributed to the improved crystallinity and particle size of brookite TiO₂. However, the sample was sintered when the calcination temperature was too high (over 500 °C), which resulted in an increased number of crystalline defects. The crystal defects correspondingly increased, thereby promoting the recombination of electrons and holes.

The semiconductor flat band potential (E_{FB}) is a fundamental thermodynamic property during interfacial electron-transfer steps. In this study, E_{FB} at the electrolyte interface of the brookite TiO₂/FTO electrode was obtained using Mott–Schottky analysis (measured in the dark); results were

then used to further investigate the intrinsic electronic properties of brookite TiO₂. The semiconductor capacitance is described using the Mott–Schottky equation:

$$1/C_{SC}^2 = 2/e_0\epsilon_0\epsilon N_D A^2 [(E - E_{FB}) - (kT/e_0)]; \quad (2)$$

where e_0 is the fundamental charge constant; ϵ is the dielectric constant of TiO₂; ϵ_0 is the permittivity of vacuum; N_D is donor density; E is the electrode applied potential, E_{FB} is the flat band potential; and kT/e_0 is the temperature-dependent correction term [38]. The Mott–Schottky plots of the brookite TiO₂/FTO electrode are presented in Fig. 7b–d. E_{FB} and

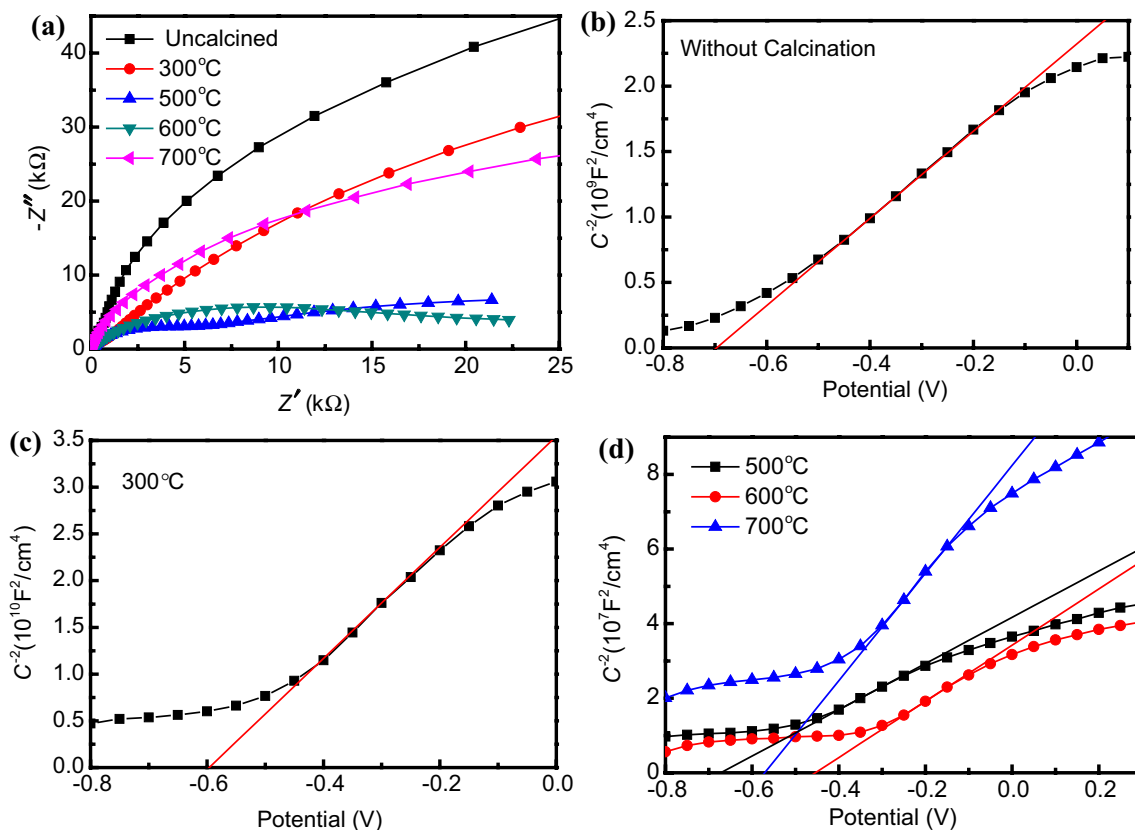


Fig. 7 a Nyquist plots, b–d Mott–Schottky plots for brookite TiO₂/FTO electrode in 0.1 mol/L Na₂SO₄ solution at 5 mV with frequency of 1000 Hz

Table 2 Flat band potentials (E_{FB}) and donor density (N_D) of brookite TiO₂ calcined at different temperatures

Calcination temperature (°C)	E_{FB} (V vs. Ag/AgCl)	E_{FB} (V vs. NHE)	N_D (cm ⁻³)
–	– 0.697	– 0.487	5.30×10^{20}
300	– 0.596	– 0.386	2.97×10^{19}
500	– 0.670	– 0.460	2.83×10^{22}
600	– 0.454	– 0.244	2.34×10^{22}
700	– 0.571	– 0.361	1.22×10^{22}

N_D are calculated from values of the x intercept and the slope of C_{SC}^2 and E , respectively. The flat band potentials of the TiO₂/FTO electrode containing brookite TiO₂ without calcination and those calcined at different temperatures are shown in Table 2. A positive shift of E_{FB} with an increase in the calcination temperature is observed due to the improvement of brookite TiO₂ crystallinity. The E_{FB} of the sample calcined at 500 °C is in good agreement with the data reported by Di Paola et al. (– 0.46 V) [39]. The donor density (N_D) is calculated via the equation $N_D = -(2/e_0\epsilon_0\epsilon)[d(1/C_{SC}^2)/dE]^{-1}$ with an ϵ value of 50 based upon the previous model. According

to the calculation in Table 2, the N_D value for brookite TiO₂ calcined at 500 °C is the highest (2.83×10^{22} cm⁻³).

To further investigate photoelectrochemical properties, the transient photocurrent of brookite TiO₂/FTO electrodes in a 0.1 mol/L Na₂SO₄ electrolyte without any sacrificial reagents or catalysts was assessed. The photocurrent response was measured at a constant bias of 0.2 V, as shown in Fig. 8. All samples were observed to have good photoresponses in the chopped light cycles. Without illumination, the current values were approximately zero. However, the photocurrent rapidly rose to a steady-state value upon illumination, which was reproducible for several on/off cycles using an approximately identical photocurrent and dark current. As the calcination temperature increased, the steady-state photocurrent first increased below 500 °C and then decreased. This is attributed to the improved charge-transfer power due to improved crystallinity.

Photocatalytic Performance Evaluation

The photocatalytic performances of brookite TiO₂ nanopowders were evaluated by photodegrading an MB solution. For comparison, a blank experiment for MB

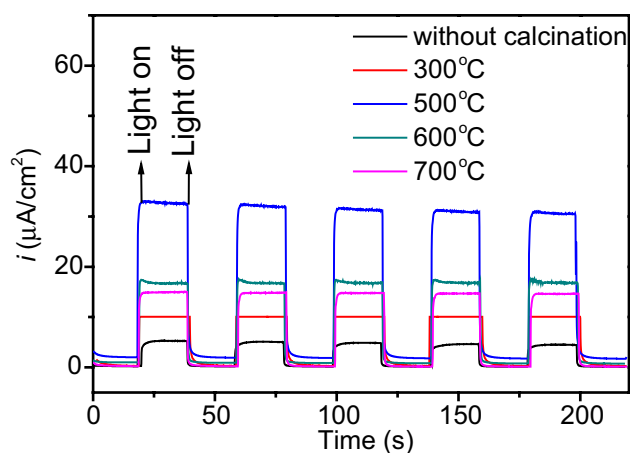


Fig. 8 Photocurrent response of TiO_2/FTO electrode at an applied potential of 0.5 V under UV light irradiation ($\lambda = 365$ nm) with 20-s light on/off cycles

photodecomposition under UV light irradiation was performed. The photocatalytic activity of P25-type TiO_2 (Degussa P25, which consists of approximately 30% rutile

and 70% anatase with a particle size of approximately 30 nm) was tested under identical conditions. Figure 9a shows that more than 90% of MB remains after UV light irradiation for 90 min in the absence of photocatalyst, which is similar to that in the presence of photocatalyst after 30 min of dark adsorption. The brookite TiO_2 sample without calcination showed a lower photoactivity (67.0%) than other samples for degradation of MB under UV irradiation. As the calcination temperature increased, the decolorization efficiency of MB firstly increased and then decreased. The sample calcined at 500 °C showed the highest decolorization efficiency of MB (approximately 96.7%) after 90 min of UV irradiation; this was higher than that of P25 (95.7%) and of the samples calcined at 300 °C (85.5%), 400 °C (95.6%), 600 °C (89.7%), and 700 °C (85.4%). In addition, the photodegradation kinetics of MB over different samples was investigated to quantitatively characterize the photocatalytic activity of the samples, from which the apparent pseudo-first-order reaction rate constants (k) were calculated (as presented in Fig. 9b). The k values of samples without thermal treatment and those calcined at 300, 500, 600 and 700 °C were 0.01172,

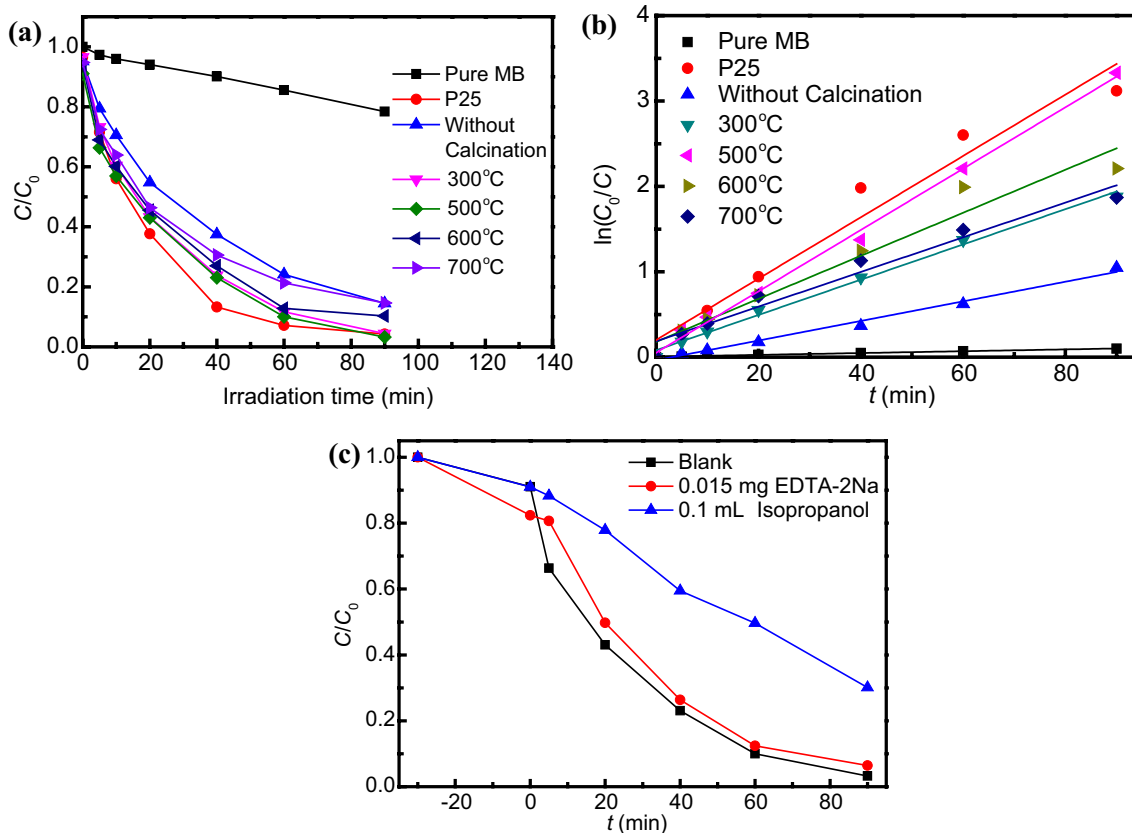


Fig. 9 **a** Photocatalytic degradation of MB under UV light irradiation of as-synthesized brookite TiO_2 without calcination and of TiO_2 calcined at different temperatures; **b** the apparent pseudo-first-order

reaction rate constants (k); **c** comparison of photocatalytic activities of sample calcined at 500 °C with addition of EDTA-2Na or 2-propanol under UV light irradiation

0.02064, 0.03592, 0.03113 and 0.0203 min⁻¹, respectively. The same results were observed for photocatalytic activity.

The photocatalytic activity of TiO₂ catalysts strongly depends on two factors: the adsorption behavior and the separation efficiency of electron-hole pairs [40–43]. Active oxygen species (such as hydroxyl radicals (OH), superoxide radicals (O₂⁻), and H₂O₂ derived from the photogenerated electrons and holes) are considered to be the major active species responsible for the photocatalytic activity of TiO₂ [40–42]. To further understand the photocatalytic mechanism of the as-synthesized brookite TiO₂, hydroxyl radicals and hole trapping experiments were designed using 2-propanol as the radical scavenger and EDTA-2Na as the holes scavenger. Results are shown in Fig. 9c, where it can be observed that the decolorization efficiency of MB with addition of EDTA-2Na is slightly smaller than that of MB with no additive. However, the decolorization efficiency of MB with addition of 2-propanol sharply decreases (65% after illumination for 90 min). This result demonstrates that ·OH is one of the major active species in this experiment and that it possesses a strong oxidation ability (its oxidation–reduction potential is + 2.27 V, vs. NHE, pH 7). It is known that ·OH radicals are generated via two pathways: (1) photoelectrons are captured by adsorbed O₂ on the surface of TiO₂ to form intermediate species, such as superoxide radicals (O₂⁻) and H₂O₂, and ·OH radicals are then generated after the series reaction; (2) the holes oxidize adsorbed water or the surface hydroxyl groups to form OH radicals [41]. Therefore, based on the result of our hole trapping experiment, we infer that superoxide radicals (O₂⁻) and H₂O₂ play important roles.

The absorption behavior is also another important factor contributing to the photocatalytic activity of TiO₂ catalysts [42–44]; the absorption behavior of organic species on the catalyst surface influences the photoinduced electron transfer, which reduces the rate of the compound cavity electronic structure and increases the photocatalytic activity. However, absorption behavior is significantly influenced by crystallinity, specific surface area, particle size, and morphology [29–33, 45–50]. Samples calcined at different temperatures had similar particle sizes and morphologies according to the XRD and SEM analyses. However, the specific surface areas and pore sizes were significantly different. Brookite TiO₂ calcined at 500 °C for 2 h had the largest specific surface area (shown in Fig. 4 and Table 1), which explains the highest photocatalytic activity. It is evident that the crystallinity of samples, which is improved after calcination at a relatively high temperature (below 500 °C), is beneficial in reducing the recombination rate of photogenerated electrons and holes (due to a decrease in the number of defects) [51].

Conclusions

In the current study, we have synthesized quasi-spherical brookite TiO₂ nanostructures via a solvothermal method in the presence of oxalic acid; a NaOH solution was introduced to maintain the pH value at approximately 10. Experimental results indicated that pure-phase brookite TiO₂ with a quasi-spherical structure was successfully synthesized under solvothermal conditions of 180 °C for 8 h. Oxalic acid played an important role in the morphology of products, and the formation of pure-phase brookite TiO₂ was attributed to the combined action of oxalic acid and the pH value, which was adjusted with sodium hydroxide. Photocatalytic activity and photoelectrochemical performance tests indicated that the resulting brookite TiO₂ nanopowders calcined at 500 °C for 2 h exhibited high photocatalytic activity for methylene blue (MB) solution, and the degradation rate of methylene blue (10 mg/L) reached 96.7% after UV light illumination for 90 min at 10 mW/cm².

Acknowledgements This work was supported by the National Key Basic Research and Development Program of China (“973” Program, No. 2012CB720100 and No. 2014CB239300), the National Natural Science Foundation of China (No. 21406164, No. 21466035 and No. 21501196) and the Science and Technology Innovation Guide Funds of Civil Aviation Administration of China (MHRD20140209). We are also grateful to the Fundamental Research Funds for the Central Universities (No. 3122016L016) and University’s Training Programs of Innovation and Entrepreneurship for Undergraduates from Civil Aviation University of China (2017).

Open Access This article is distributed under the terms of the Creative Commons Attribution 4.0 International License (<http://creativecommons.org/licenses/by/4.0/>), which permits unrestricted use, distribution, and reproduction in any medium, provided you give appropriate credit to the original author(s) and the source, provide a link to the Creative Commons license, and indicate if changes were made.

References

1. Bokhimi X, Morales A, Aguilar M et al (2001) Local order in titania polymorphs. *Int J Hydrog Energy* 26(12):1279–1287
2. Kumar SG, Rao KSRK (2014) Polymorphic phase transition among the titania crystal structures using a solution-based approach: from precursor chemistry to nucleation process. *Nanoscale* 6(20):11574–11632
3. Kumar SG, Devi LG (2011) Review on modified TiO₂ photocatalysis under UV/Visible light: selected results and related mechanisms on interfacial charge carrier transfer dynamics. *J Phys Chem A* 115(46):13211–13241
4. Koelsch M, Cassignon S, Guillemoles JF et al (2002) Comparison of optical and electrochemical properties of anatase and brookite TiO₂ synthesized by the sol–gel method. *Thin Solid Films* 403–404(2):312–319
5. Di Paola A, Bellardita M, Palmisano L (2013) Brookite, the least known TiO₂ photocatalyst. *Catalysts* 3(1):36–73

6. Di Paola A, Addamo M, Bellardita M (2007) Preparation of photocatalytic brookite thin films. *Thin Solid Films* 515(7):3527–3529
7. Gong XQ, Selloni A (2007) A first-principles study of the structures and energetics of stoichiometric brookite TiO_2 surfaces. *Phys Rev B* 76(23):235307–235317
8. Lin HF, Li LP, Zhao ML et al (2012) Synthesis of high-quality brookite TiO_2 single-crystalline nanosheets with specific facets exposed: tuning catalysts from inert to highly reactive. *J Am Chem Soc* 134(20):8328–8331
9. Kobayashi M, Petrykin V, Tomita K et al (2011) Hydrothermal synthesis of brookite-type titanium dioxide with snowflake-like nanostructures using a water-soluble citratoperoxotitanate complex. *J Cryst Growth* 337(1):30–37
10. Morishima Y, Kobayashi M, Petrykin V et al (2009) Hydrothermal synthesis of brookite type TiO_2 photocatalysts using a water-soluble Ti-complex coordinated by ethylenediaminetetraacetic acid. *J Ceram Soc Jpn* 117(1363):320–325
11. Ohno Y, Tomita K, Komatsubara Y et al (2011) Pseudo-cube shaped brookite (TiO_2) nanocrystals synthesized by an oleate-modified hydrothermal growth method. *Cryst Growth Des* 11(11):4831–4836
12. Katsumata K, Ohno Y, Tomita K et al (2012) Synthesis of amphiphilic brookite nanoparticles with high photocatalytic performance for wide range of application. *ACS Appl Mater Interfaces* 4(9):4846–4852
13. Hall SR, Swinerd VM, Newby FN et al (2006) Fabrication of porous titania (brookite) microparticles with complex morphology by sol-gel replication of pollen grains. *Chem Mater* 18(3):598–600
14. You YF, Xu CH, Xu SS et al (2014) Structural characterization and optical property of TiO_2 powders prepared by the sol-gel method. *Ceram Int* 40(6):8659–8666
15. Dambournet D, Belharouak I, Ma JW et al (2011) Toward high surface area TiO_2 brookite with morphology control. *J Mater Chem* 21(9):3085–3090
16. Kominami H, Ishii Y, Kohno M et al (2003) Nanocrystalline brookite-type titanium(IV) oxide photocatalysts prepared by a solvothermal method: correlation between their physical properties and photocatalytic activities. *Catal Lett* 91(1–2):41–47
17. Zhao YB, Pan F, Li H et al (2013) Uniform mesoporous anatase-brookite biphasic TiO_2 hollow spheres with high crystallinity via Ostwald ripening. *J Phys Chem C* 117(42):21718–21723
18. Kobayashi M, Tomita K, Petrykin V et al (2008) Direct synthesis of brookite-type titanium oxide by hydrothermal method using water-soluble titanium complexes. *J Mater Sci* 43(7):2158–2162
19. Truong QD, Le TH, Liu JY et al (2012) Synthesis of TiO_2 nanoparticles using novel titanium oxalate complex towards visible light-driven photocatalytic reduction of CO_2 to CH_3OH . *Appl Catal A Gen* 437–438(5):28–35
20. Kominami H, Kohno M, Kera Y (2000) Synthesis of brookite-type titanium oxide nano-crystals in organic media. *J Mater Chem* 10(5):1151–1156
21. Tomita K, Petrykin V, Kobayashi M et al (2006) A water-soluble titanium complex for the selective synthesis of nanocrystalline brookite, rutile, and anatase by a hydrothermal method. *Angew Chem Int Ed* 45(15):2378–2381
22. Dambournet D, Belharouak I, Amine K (2010) Tailored preparation methods of TiO_2 anatase, rutile, brookite: mechanism of formation and electrochemical properties. *Chem Mater* 22(3):1173–1179
23. Boudaren C, Bataille T, Auffrédic J et al (2003) Synthesis, structure determination from powder diffraction data and thermal behaviour of titanium (IV) oxalate $[\text{Ti}_2\text{O}_3(\text{H}_2\text{O})_2](\text{C}_2\text{O}_4)\cdot\text{H}_2\text{O}$. *Solid State Sci* 5:175–182
24. Shang QQ, Tan X, Yu T et al (2015) Efficient gaseous toluene photoconversion on grapheme-titanium dioxide nanocomposites with dominate exposed 001 facets. *J Colloid Interf Sci* 455:134–144
25. Zhao B, Lin L, He DN (2013) Phase and morphological transitions of titania/titanate nanostructures from an acid to an alkali hydrothermal environment. *J Mater Chem A* 1(5):1659–1668
26. Tompsett GA, Bowmaker GA, Cooney RP et al (1995) The Raman spectrum of brookite, TiO_2 (*Pbca*, $Z = 8$). *J Raman Spectrosc* 26(1):57–62
27. Iliev MN, Hadjiev VG, Litvinchuk AP (2013) Raman and infrared spectra of brookite (TiO_2): experiment and theory. *Vib Spectrosc* 64(1):148–152
28. Zhang H, Banfield J (1998) Thermodynamic analysis of phase stability of nanocrystalline titania. *J Mater Chem* 8(9):2073–2076
29. Jolivet JP (2000) Metal oxide chemistry and synthesis: from solution to solid state. Wiley, New York
30. Kanna M, Wongnawa S (2008) Mixed amorphous, nanocrystalline TiO_2 powders prepared by sol-gel method: characterization and photocatalytic study. *Mater Chem Phys* 110(1):166–175
31. Yu JG, Yu HG, Cheng B et al (2003) The effect of calcination temperature on the surface microstructure and photocatalytic activity of TiO_2 thin films prepared by liquid phase deposition. *J Phys Chem B* 107(50):13871–13879
32. Liu CP, Yu T, Tan X (2016) Characterization and photocatalytic activity of mixed nanocrystalline TiO_2 powders prepared by xerogel-hydrothermal method in different acid solutions. *Trans Tianjin Univ* 22(5):473–479
33. Yin S, Hasegawa H, Maeda D et al (2004) Synthesis of visible-light-active nanosize rutile titania photocatalyst by low temperature dissolution-reprecipitation process. *J Photochem Photobiol A Chem* 163(1):1–8
34. Yang HY, Chen F, Jiao YC et al (2013) Investigation of phase transitions for the hydrothermal formation of TiO_2 in the presence of F^- ions. *Chem Eng J* 214(4):229–236
35. Djaoued Y, Thibodeau M, Robichaud J et al (2008) Photocatalytic degradation of domoic acid using nanocrystalline TiO_2 thin films. *J Photochem Photobiol A Chem* 193(2–3):271–283
36. Di Paola A, Cufalo G, Addamo M et al (2008) Photocatalytic activity of nanocrystalline TiO_2 (brookite, rutile and brookite-based) powders prepared by thermohydrolysis of TiCl_4 in aqueous chloride solutions. *Colloids Surf A* 317(1–3):366–376
37. Prieto-Mahaney O, Murakami N, Abe R et al (2009) Correlation between photocatalytic activities and structural and physical properties of titanium (IV) oxide powders. *Chem Lett* 38(3):238–239
38. Wang J, Zhang WD (2012) Modification of TiO_2 nanorod arrays by graphite-like C_3N_4 with high visible light photoelectrochemical activity. *Electrochim Acta* 71(3):10–16
39. Di Paola A, Bellardita M, Ceccato R et al (2009) Highly active photocatalytic TiO_2 powders obtained by thermohydrolysis of TiCl_4 in water. *J Phys Chem C* 113(34):15166–15174
40. Xiao Q, Si ZC, Zhang J et al (2008) Photoinduced hydroxyl radical and photocatalytic activity of samarium-doped TiO_2 nanocrystalline. *J Hazard Mater* 150(1):62–67
41. Ishibashi K, Fujishima A, Watanabe T et al (2000) Detection of active oxidative species in TiO_2 photocatalysis using the fluorescence technique. *Electrochem Commun* 2(3):207–210
42. Choi M, Yong K (2014) A facile strategy to fabricate high-quality single crystalline brookite TiO_2 nanoarrays and their photoelectrochemical properties. *Nanoscale* 6(22):13900–13909
43. Hoffmann MR, Choi ST, Martin W et al (1995) Environmental applications of semiconductor photocatalysis. *Chem Rev* 95(1):69–96
44. Liu H, Cheng SA, Wu M et al (2000) Photoelectrocatalytic degradation of sulfosalicylic acid and its electro-chemical impedance spectroscopy investigation. *J Phys Chem A* 104(30):7016–7020

45. Linsebigler AL, Lu G, Yates JT (1995) Photocatalysis on TiO₂ surfaces: principles, mechanisms, and selected results. *Chem Rev* 95(3):735–758
46. Liu G, Wang XW, Wang LZ et al (2009) Drastically enhanced photocatalytic activity in nitrogen doped mesoporous TiO₂ with abundant surface states. *J Colloid Interface Sci* 334(2):171–175
47. Zhao B, Chen F, Huang QW et al (2009) Brookite TiO₂ nanoflowers. *Chem Commun* 34(34):5115–5117
48. Verma A, Samanta SB, Bakhshi AK et al (2005) Effect of stabilizer on structural, optical and electrochemical properties of sol-gel derived spin coated TiO₂ films. *Sol Energy Mater Sol Cells* 88(1):47–64
49. Xiang Q, Yu J, Wong PK (2011) Quantitative characterization of hydroxyl radicals produced by various photocatalysts. *J Colloid Interface Sci* 357(1):163–167
50. Lin HX, Wang XX, Fu XZ (2007) Properties and distribution of the surface hydroxyl groups of TiO₂. *Prog Chem* 19(5):665–670
51. Hao H, Zhang J (2009) Low temperature synthesis of crystalline mesoporous titania with high photocatalytic activity by post-treatment in nitric acid ethanol solution. *Mater Lett* 63(1):106–108